NASA DEVELOP National Program
Alabama – Marshall

Summer 2020

Huntsville Urban Development

Utilizing NASA Earth Observations to Evaluate Urban Tree Canopy and Land Surface Temperature for Green Infrastructure Development and Urban Heat Mitigation in Huntsville, AL

DEVELOP Technical Report
Final Draft – August 6th, 2020

Greta Paris (Project Lead)
Sabine Nix
Thomas Quintero
Amanda Tomlinson

Advisors
Dr. Robert Griffin, The University of Alabama in Huntsville (Science Advisor)
Dr. Jeffrey Luvall, NASA Marshall Space Flight Center (Science Advisor)

1. Abstract

Huntsville, Alabama's population has grown by approximately 11% since 2010, due in part to the city's advancing engineering industry. Rapid urban growth negatively impacts the environment by decreasing tree canopy cover and increasing impervious surface cover, which can intensify the urban heat island effect. To examine the impacts of this urban growth on the environment, the team partnered with the City of Huntsville to utilize Landsat 5 Thematic Mapper (TM), Landsat 8 Operational Land Imager (OLI) and Thermal Infrared Sensor (TIRS), Terra Moderate Resolution Imaging Spectroradiometer (MODIS) and the International Space Station's Global Ecosystems Dynamic Investigation (GEDI) and ECOsystem Spaceborne Thermal Radiometer Experiment on Space Station (ECOSTRESS). The team utilized these Earth observations in combination with ancillary datasets to create a suite of end products to assist in mitigating the effects of extreme heat due to urban expansion and tree canopy loss. Annual land surface temperature (LST) was calculated and land cover classes were derived through supervised and threshold classification methods to distinguish trees, other vegetation types, impervious surfaces, and water. From 2010 to 2019, LST increased approximately 4 °F for all census tracts within the city and the total amount of tree cover increased by approximately 3%. The findings will aid the city in future decision-making processes by indicating areas that would benefit from increased green infrastructure.

Key Terms
Landsat, GEDI, urban heat island, urban expansion, remote sensing, NDVI, NDBI, urban forestry

2. Introduction

2.1 Background Information

Urban heat islands (UHIs) are caused by urban development involving the replacement of forested areas with impervious surfaces, such as asphalt or concrete, which increases the temperature of urban areas relative to their surroundings (Lo et al., 1997). Warmer temperatures increase the amount of volatile organic compounds emitted from car exhaust, elevating air pollution levels within cities experiencing the UHI effect. Higher temperatures catalyze chemical reactions forming ozone, which has been found to cause lung inflammation and aggravate respiratory conditions (Stone & Rogers, 2001). Those over the age of 65 and those living in older homes are also vulnerable to heat-related illnesses (Reid et al., 2012).

To protect the health and safety of their populations, many cities look to green infrastructure and tree planting to mitigate the UHI effect. The Environmental Protection Agency (EPA) suggests that green infrastructure can mitigate effects from urban heat by releasing moisture into the atmosphere and increasing surface reflectance to combat solar radiation (EPA, 2015). Urban tree cover is especially important because trees play a large role in mitigating the UHI effect (Nowak, 2007; Ossola & Hopton, 2018). Trees are effective at reducing temperatures through evapotranspiration and casting shade on nearby surfaces and buildings. A study done by Kravcík et al. (2009) found that on a sunny day, the evapotranspiration of a tree can cool an area with a power equal to 20-30 kW,

which is comparable to more than ten air-conditioners (Kleerekoper et al., 2012). This evidence suggests that trees have significant impacts on cooling environments, making tree planting an important part of mitigating the UHI effect.

Researchers and city officials are interested in identifying hotspots of urban heat as well as mitigation strategies. While heat can be measured from the ground, remotely sensed data, including Earth observations (EOs), offer researchers the ability to look at temperatures across an entire city rather than at a few points. Satellite sensors such as Landsat 8 Thermal Infrared Spectrometer (TIRS), Aqua and Terra Moderate Resolution Spectroradiometer (MODIS), as well as airborne Light Detection and Ranging (LiDAR), detect information in thermal infrared sections of the electromagnetic spectrum and have been used successfully to calculate land surface temperature (LST) across urban areas (Lo & Luvall, 1997; Imhoff et al., 2010; Keeratikasikorn & Bonafoni, 2018). The increasing accessibility of LiDAR gives cities new opportunities to use this data for their urban planning initiatives. The International Space Station's (ISS) Global Ecosystem Dynamics Investigation (GEDI) is one example of an instrument that obtains LiDAR data of nearly the entirety of Earth's surface (Dubayah et al., 2020). In cases where high resolution maps of land cover are not available, indices such as the Normalized Difference Vegetation Index (NDVI) and the Normalized Difference Built-Up Index (NDBI) can be used to examine the relationship between land cover and the UHI effect (Lo & Luvall, 1997; Grover & Singh, 2015; Zhang et al., 2009; Macarof & Statescu, 2017).

Huntsville, Alabama, served as the study area for this project, and the team focused on the summer months of June to August from 2010 to 2019 (*Figure 1*). Huntsville represents an ideal city to study the UHI effect due to its rapid urban development that stems from a booming space economy. With a population growth rate of 10.8% from 2010 to 2019, Huntsville is growing at a rate double that of the national average (City of Huntsville Urban Development, Long-Range Planning Division, 2020). The University of Alabama's Center for Business and Economic Research (CBER; 2020) predicts a population increase of 26.5% between 2010 and 2030.

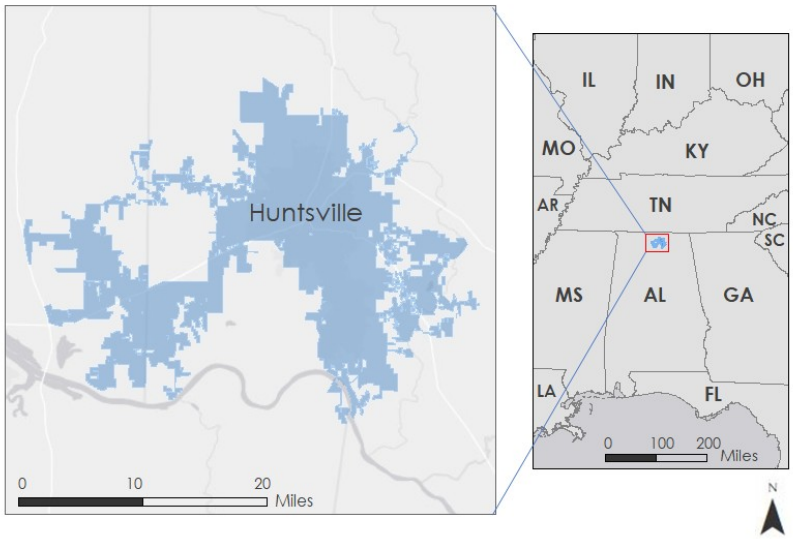

Figure 1. This map shows the extent of the city of Huntsville in North Alabama.

2.2 Project Partners & Objectives

The team partnered with the City of Huntsville and worked with several departments including the City Council, Urban and Long-Range Planning, Geographic Information Systems (GIS) Department, City Planning, City Engineering, and Landscape Management. The city's major interest comes from its constituents who expressed concern over the loss of trees, which effect the temperature. The City of Huntsville wanted to investigate whether there was a correlation between tree cover and temperature, and thus the presence of an UHI. The products created will help the City of Huntsville identify where UHIs might exist and allow them to focus tree planting efforts in these areas. The City of Huntsville currently does not hold the capacity to use EOs, so this project helped to increase the amount and range of data supporting their decision-making processes.

To address these concerns, the team's main objective involved quantifying the impact of Huntsville's urban expansion on the loss of the city's tree canopy cover and the resulting UHI effect. The team also assessed the relationship between factors of heat vulnerability, tree canopy cover, expansion of impervious surfaces, and LST. To assess heat vulnerability in Huntsville, the team looked at populations that would be most sensitive to intensified heat, including the percentage of people per census tract over the age of 65 or with conditions such as asthma, diabetes, cardiovascular issues, or pulmonary issues.

3. Methodology

3.1 Data Acquisition

3.1.1 Land Cover (NDVI and NDBI)

To create land cover maps, the team obtained Landsat 5 Surface Reflectance Tier 1 scenes from the Thematic Mapper (TM) instrument and Landsat 8 Surface Reflectance Tier 1 scenes from the Operational Land Imager (OLI) and Thermal Infrared Sensor (TIRS) instrument and imported them into Google Earth Engine (GEE). Due to the UHI effect being enhanced and most dangerous during the summer (Imhoff et al., 2010), the team chose to narrow the study period to the meteorological definition of summer (June 1st to August 31st). The team acquired images between June 1st and August 31st from 2010 to 2011 (Landsat 5 TM), and 2013 to 2019 (Landsat 8 OLI and TIRS) for processing. For the bands utilized to calculate NDVI and NDBI, the Landsat imagery has a spatial resolution of 30 m (Table 1).

Table 1
Satellites used to create LST, NDVI, and NDBI time-series maps.

Satellite	Years	Parameter	Bands	Resolution
Landsat 5 TM	2010-2011	NDVI, NDBI	Band 3 (red), Band 4 (near-infrared), Band 5 (shortwave-infrared 1)	30m
		LST	Band 6 (brightness	120m

			temperature (BT))	
Landsat 8 OLI & TIRS	2013-2019	NDVI, NDBI	Band 4 (red), Band 5 (near-infrared), Band 6 (shortwave-infrared 1)	30m
		LST	Band 10 (BT)	100m

In addition to the EO imagery, the team imported the United States Geological Survey's (USGS) National Land Cover Database (NLCD) from the Multi-Resolution Land Characteristics Consortium website (Homer et al., 2020). To aid in classifying land cover and determining appropriate NDVI and NDBI thresholds between 2010 and 2019, the team downloaded both the 2011 and 2016 NLCD data. The NLCD data are based on Landsat imagery and have a resolution of 30 m.

3.1.2 Land Surface Temperature (LST)

To calculate LST, the team utilized the same Landsat 5 TM and Landsat 8 OLI and TIRS imagery described above in section 3.1.1 within GEE. Band 6 in Landsat 5 TM and Band 10 in Landsat 8 OLI and TIRS were utilized to calculate LST and the images have a spatial resolution of 120m and 100m, respectively. Details of the imagery utilized to calculate LST, NDVI, and NDBI are included in Table 1.

3.1.3 Heat Vulnerability Variables

To study the varying effects of UHIs on urban populations, the team utilized socioeconomic and health data at the census block level. The team queried socioeconomic data, including the percent of the population over 65, from the 2018 American Community Survey five-year estimates for the city of Huntsville. The team sourced epidemiological data from 2018, including information on diabetes, asthma, cardiovascular illnesses, and pulmonary illnesses from the Center for Disease Control's (CDC) data hub. Our team acquired these data by using an existing R code created by the NASA DEVELOP Spring 2020 Philadelphia Health & Air Quality Team and modified it to retrieve data for Huntsville. To study these heat vulnerability variables at the census block level, the team downloaded the Topologically Integrated Geographic Encoding and Referencing shapefiles of the City of Huntsville's census tracts from the City of Huntsville GIS Department's public data hub and imported the data into GEE for processing the LST, NDVI, and NDBI at the census block level.

3.1.4 Tree Canopy Cover

The GEDI instrument aboard the ISS takes high resolution laser ranging measurements of Earth's forests and topography. GEDI's lasers pulse 242 times per second and each measurement covers nearly 25 m^2 of ground surface (Dubayah, 2020). The team downloaded GEDI Level 2B data from NASA's Earthdata Search specifying a region of interest around Huntsville. These products contain vegetation biophysical variables such as canopy height, total canopy cover, and plant area index (Earthdata Search, 2019). The dates of acquisition for the data are between May 18, 2019 to September 20, 2019. Plant area index is a measurement of leaf area index across the entire plant. Leaf area index is a ratio of how many layers of vegetation cover its cross-sectional area on the ground. For

example, a plant with a leaf area index of two has two leaves which cover the ground surface below those leaves.

3.1.5 UHI Identification

The team obtained average LST for the City of Huntsville in 2019 from Landsat 8 TIRS for the summer months of June-August as outlined in section 3.1.2. Our team used average LST for 2019 to identify areas throughout the study area exhibiting potential UHI effect. The team obtained ISS ECOsystem Spaceborne Thermal Radiometer Experiment on Space Station (ECOSTRESS) ECO2LSTE LST layer from the USGS Application for Extracting and Exploring Analysis Ready Samples (AppEEARS) database for June 12th, 2020. The team also downloaded the nighttime LST product from Terra Moderate Resolution Spectroradiometer (MODIS) MOD11A1 nighttime LST layer from USGS AppEEARS for June 12th 2020 for a day and nighttime LST comparison.

3.2 Data Processing

3.2.1 Land Cover (NDVI and NDBI)

Once imported into GEE, the team clipped all images to the study area with a polygon slightly larger than the City of Huntsville boundary. Next, the team added a cloud mask within GEE to the images from Landsat 5 TM and Landsat 8 OLI. In order to determine how trees and other vegetation are distributed throughout the city, the team calculated NDVI for each image acquired between 2010 and 2019 (Equation 1). The team excluded the year 2012 from the study period due to image striping issues with Landsat 7 Enhanced Thematic Mapper Plus.

$$\mathrm{NDVI} = \frac{\mathrm{NIR} - \mathrm{Red}}{\mathrm{NIR} + \mathrm{Red}} \tag{1}$$

The team utilized NDBI to determine the distribution of impervious surfaces throughout the city (Equation 2). Our team calculated NDBI from each image acquired between 2010 and 2019 (excluding 2012).

$$\mathrm{NDBI} = \frac{\mathrm{SWIR} - \mathrm{NIR}}{\mathrm{SWIR} + \mathrm{NIR}} \tag{2}$$

For each index and for each year, the team combined images by calculating the mean of each pixel to produce a single image for NDVI and NDBI for each summer within the study period. Combining the images allowed us to reduce areas of missing data due to cloud masking. The team visually checked each image for large areas of missing data before downloading it for use in analysis. The team also created a set of LST maps averaged over census blocks for use in statistical analyses and to facilitate comparison with heat vulnerability variables, which are available at the census block level.

After calculating NDVI and NDBI, the team utilized the NLCD to determine appropriate thresholds to classify tree cover, vegetation, impervious cover, and water from the NDVI and NDBI images. Using ArcGIS Pro 2.5, the team determined the minimum, maximum, mean, and standard deviation pixel values for NDVI and NDBI values within each land cover class as defined by the NLCD 2016 data. Based on the ranges of pixel values associated with each NLCD land cover class, the team then assigned NDVI and NDBI thresholds to each class. The thresholds for each land cover class are described in Table 2 below.

Table 2
NDVI thresholds used to classify land cover types.

Land Cover Class	NDVI Threshold Values
Tree Cover	Greater than 0.75
Pervious Cover	0.60 - 0.75
Developed / Impervious Cover	0.00 - 0.60
Water	Less than 0.00

The team utilized these thresholds within GEE to classify NDVI and NDBI images into the land cover classes described above. To assess the accuracy of these classifications, the team manually determined the correct land cover class for 150 randomly selected points across the study area. To determine the correct land cover class at each point, the team referenced the United States Department of Agriculture's (USDA) National Agriculture Imagery Program (NAIP) imagery for 2011 and 2017. The team created confusion matrices for 2011, 2016, and 2017 to assess the accuracy of our threshold classifications using the manually classified NAIP imagery for 2011 and 2017, and the NLCD data for 2011 and 2016 (Appendix A).

After completing the threshold classification and calculating the accuracies, the team conducted a supervised classification based directly on the Landsat 5 TM and Landsat 8 OLI images using the NLCD data as training data. To create a more targeted classification, the team remapped the NLCD land cover classes to focus on classes of interest to the partners. The team classified the study area into four classes: tree cover, developed/impervious cover, water, and other pervious cover. Other pervious cover includes non-tree vegetation, such as lawns, grasses, and agricultural fields, as well as non-vegetated pervious land cover such as barren soil. As for the threshold classifications, the team created confusion matrices based on manually classified points for 2011 and 2017, as well as the NLCD data for 2011 and 2016 (Appendix A).

3.2.2 Land Surface Temperature (LST)
To calculate LST, the team utilized the NDVI images to calculate emissivity (E) for each year (Shen et al., 2016), as well as the BT bands on Landsat 5 TM (Band 6) and Landsat 8 TIRS. The equation for LST is shown below (Equation 3). The team calculated LST within GEE using a script adapted from the NASA DEVELOP Fall 2019 Louisville Urban Development project at the Arizona-Tempe Node.

$$\mathrm{LST} = \frac{\mathrm{BT}}{\left(1 + \left(0.0000115 * \left(\frac{\mathrm{BT}}{0.01438}\right) * \log(\mathrm{E})\right)\right)} \quad (3)$$

As with NDVI and NDBI, the team calculated LST on each image acquired for the years between 2010 and 2019, and then combined the images by calculating the median for each pixel to create one final LST image for each year. The team also created a set of LST images averaged over census tracts for use in statistical analyses and to facilitate comparison with heat vulnerability variables, which were downloaded at the census tract level.

3.2.3 Heat Vulnerability Variables
The team utilized an existing R script created by the Spring 2020 Philadelphia Health & Air Quality DEVELOP team to calculate a Heat Vulnerability Index (HVI). The team loaded the LST, NDVI, and NDBI values averaged over each census tract along with the percentage of the population in each tract with the previously identified medical conditions into R Studio 1.3.959 running R 4.0.0. Next, the team performed three separate Principal Component Analyses (PCA). The first PCA used the environmental variables to calculate a Heat Exposure Index (HEI). The second PCA used the health and census data to calculate a Heat Sensitivity Index (HSI). Lastly, the team performed the third and final PCA in which the team combined the HEI and HSI to calculate the overall HVI.

3.2.4 Tree Canopy Cover Survey
The team converted GEDI Level 2B data into a shapefile using Silva et al.'s rGEDI package (2020) and imported them into ArcGIS Pro 2.5. Next, the team filtered the GEDI points so that they passed the instrument derived quality check mask and had over 40% tree cover. The quality of the image is calculated by whether or not the LiDAR transect passed over a cloud upon scanning. Each acquisition point determines tree cover using MODIS and Landsat imagery at the time of original data acquisition.

3.2.5 UHI Identification
The team processed average LST for 2019 with Landsat 8 TIRS data using the methods stated in section 3.2.2. Next, the team loaded this dataset into ArcMap 10.5.1 and layered the City of Huntsville Census tracts over top to spatially demonstrate LST throughout the city. Then, the team loaded the ISS ECOSTRESS ECO2LSTE data for June 12, 2020 into ArcMap 10.5.1 and converted LST values from Kelvin to Fahrenheit. The team loaded the Terra MODIS MOD11A1 nighttime LST data for June 12, 2020 into ArcMap 10.5.1 and repeated the previous steps used for the ECOSTRESS data to process nighttime LST. Lastly, the team clipped both the daytime and nighttime LST rasters to a rectangular region of interest around the city of Huntsville boundaries, and overlaid a shapefile of City of Huntsville census tracts was to observe LST throughout the city.

3.3 Data Analysis
3.3.1 Land Surface Temperature and Land Cover Change
The team compared the tree canopy change map with the LST change map by first quantifying the percent change of the two factors per census tract. The team then conducted a bivariate regression analysis to determine general correlation and plotted the data in Excel. After joining the percent change data to the census tract shapefile, the team ran an ordinary least squares (OLS) regression in ArcGIS Pro to visualize where census tracts were above or below the expected tree canopy development given surface temperature. Following the OLS regression, the team conducted a Moran's I spatial auto-correlation test to determine if a spatially corrected model was necessary such as a Spatial Autoregression (SAR) model. The team then ran the local bivariate relationships tool to visualize where tree canopy growth and land surface temperature were positively or negatively correlated.

3.3.2 Tree Canopy Cover Survey

The team exported the LiDAR return points from ArcGIS Pro to run descriptive statistics on the GEDI points representative of the local tree canopy. The team then extracted and graphed properties such as the mean tree canopy height and plant area index because they showed the present range and distribution of values. Finally, to visualize the role that trees play on reducing LST, the team created 3D ArcScene maps to display the GEDI data on a smaller scale.

4. Results & Discussion

4.1 Analysis of Results

4.1.1 Land Surface Temperature and Land Cover Change

Based on the confusion matrices produced for both the threshold classifications and supervised classifications (Appendix A), the team determined that the supervised classifications had higher overall accuracy and should be used for analysis of land cover change. The team looked specifically at tree cover and impervious cover due to the partner's interest in identifying areas of potential tree cover loss due to urban expansion. Overall, the team found that the percent tree canopy cover increased from 22.7% in 2010 to 26.1% in 2019 within the city limits. Impervious surface cover, on the other hand, stayed relatively constant near 20.5% for both 2010 and 2019 (Table 3). These results suggest that Huntsville's urban development likely has not contributed to a substantial loss in tree cover or increase in impervious surfaces within the city boundary. These values do not take into account changes occurring beyond the city boundary, which may be developing more rapidly as Huntsville's population grows. It is important to note also that the changes noted in Table 3 may be within the range of error as described by our confusion matrices.

Table 3
Land cover changes between 2010 and 2019 within Huntsville's City Limits.

Year	**2010**	**2019**
Tree Cover (%)	22.7	26.1
Pervious Cover (%)	53.4	50.2
Impervious Cover (%)	20.7	20.5

The team also conducted a series of analyses and statistical tests for the land cover and LST data averaged over census tracts to better understand where the largest changes have occurred throughout the city and which tracts should be prioritized for UHI mitigation efforts. When averaged over census tracts, the land cover data from the supervised classifications indicated that while most census tracts had relatively stable or increasing tree canopy cover percentages between 2010 and 2019, some tracts saw losses of up to 4% tree cover (Figure 2).

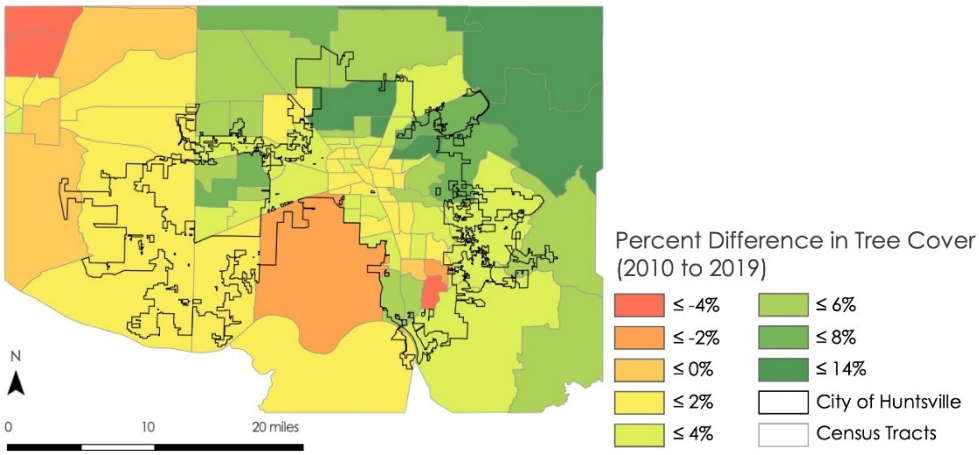

Figure 2. Percent Tree Cover Change by Census Tracts, 2010 –2019.

While these results effectively demonstrate the changes in land cover between years, they cannot indicate which land cover classes are being converted into each other. To better understand whether changes in impervious surfaces are directly leading to tree cover loss or pervious surface loss, the team created a Sankey diagram using the supervised classification data from 2010 and 2019 (Figure 3). As demonstrated in Figure 3 below, the team found that the minimal amount of tree cover that is converted into impervious surface is matched by the amount of impervious surface that becomes tree cover, suggesting that Huntsville's urban development has not led to a substantial portion of tree cover being converted to impervious surfaces. Instead, it appears that much of Huntsville's expansion has been occurring in open fields or other pervious land.

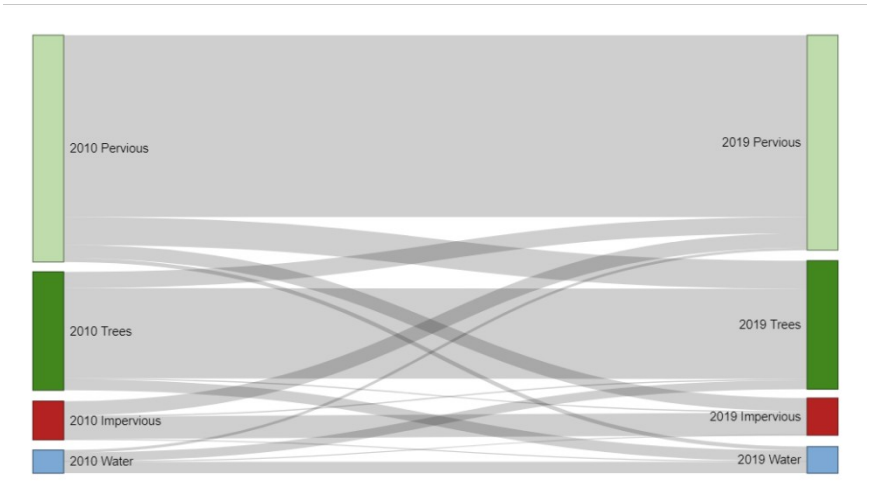

Figure 3. Sankey plot displaying the change of land cover classes between 2010 and 2019.

The team also averaged the LST data over census tracts to facilitate comparison with census tract level health data and land cover data. Overall, between 2010 and 2019 the team found that LST increased by 4 °F across the entire study area, with some tracts seeing increases as high as 8°F. Notably, every census tract in the study area saw an increase in LST between 2010 and 2019 (Figure 4).

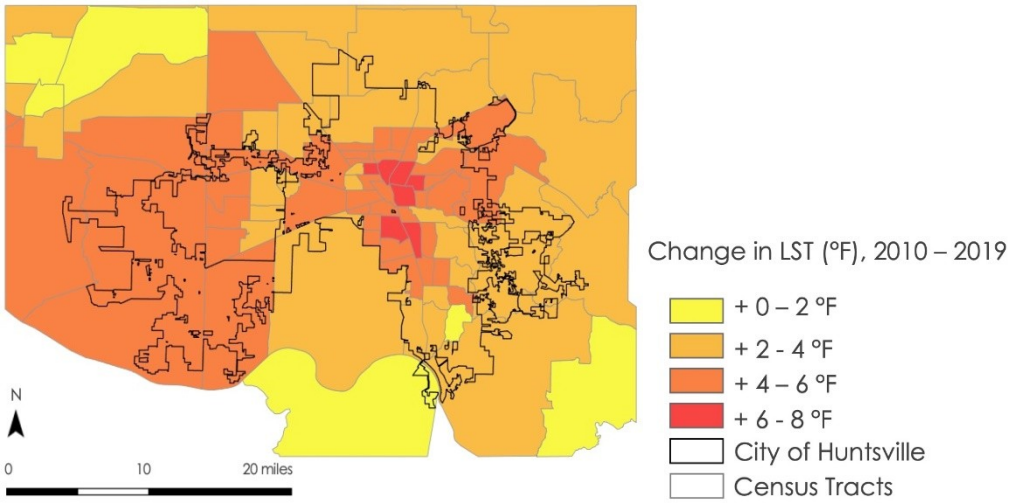

Figure 4. Change in LST by Census Tracts, 2010-2019.

The OLS regression produced residuals that our team tested for spatial autocorrelation with the Moran's I test using an R script. The residuals did spatially correlate, so a SAR model was necessary. The team conducted a SAR model to test how well tree cover and impervious cover explain LST (Appendix B). An appropriate SAR test was chosen through a series of Lagrange tests to identify the most significant p-value. The team chose an error-corrected SAR model that produced a pseudo R^2 value of 0.9 calculated from an AIC of 234.8 and had a p-value of < 2.2e-16. While both tree cover (p = 3.8e-09) and developed area (p < 2.2e-16) explain LST very well, developed area more definitely explains changes in LST because it has a lower p-value in the SAR model. This model also confirms that tree cover and LST are negatively correlated (LST decreases 1°F for every 14.1% increase in tree cover) and developed area and LST are positively correlated (LST increases 1°F for every 7.3% increase in developed area cover).

After discovering that the data were spatially autocorrelated, the team ran a multivariate clustering analysis using tree cover, impervious cover, and LST as the variables. The team discovered four distinct clusters (Figure 5). The resultant map shows Cluster 1 (moderately low tree cover, moderately high developed area, and moderately high LST), Cluster 2 (moderate tree cover, moderately low developed area, and moderately low LST), Cluster 3 (very low tree cover, very high developed area, and very high LST), and Cluster 4 (very high tree cover, very low developed area, and very low LST).

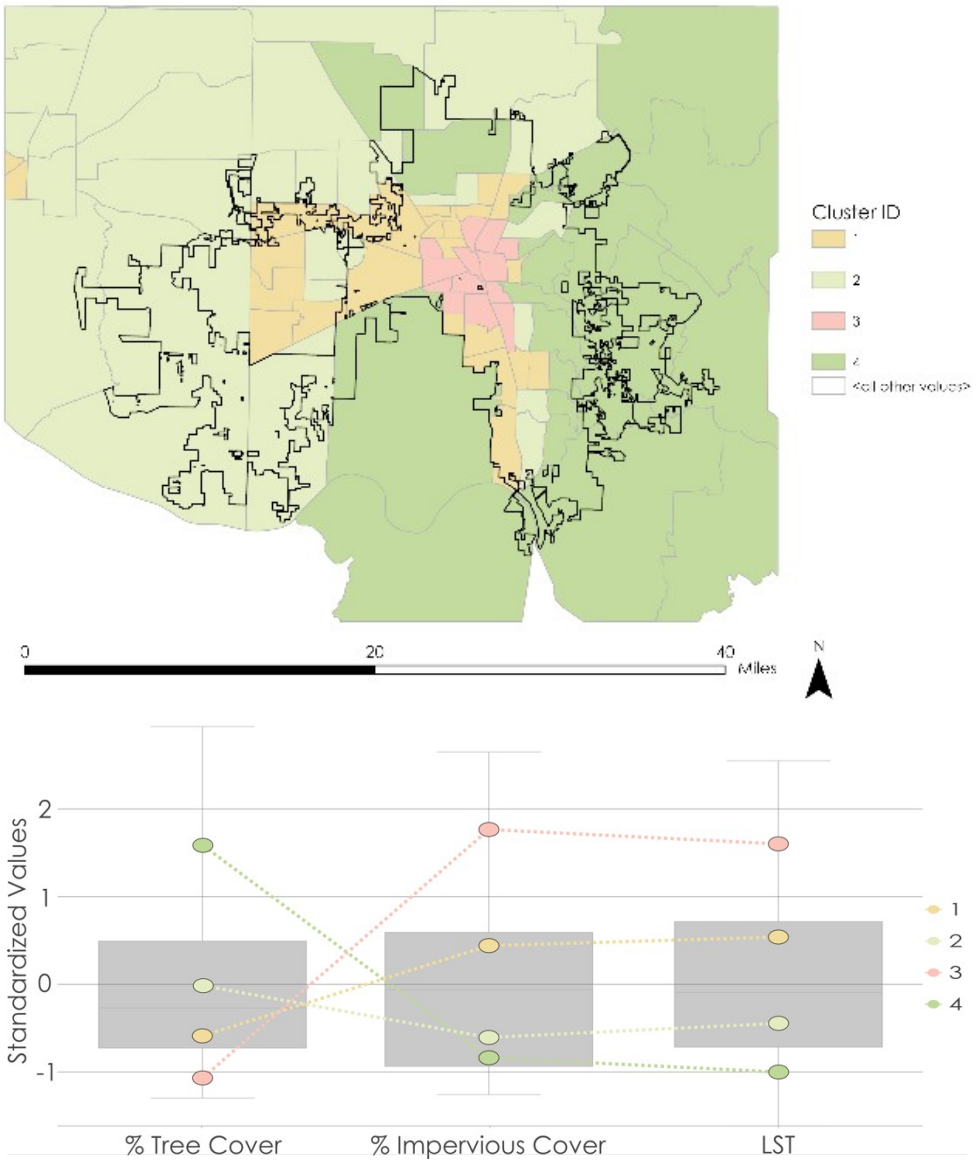

Figure 5. Multivariate clustering map (top) and explanatory box plots (bottom) for 2019.

Local bivariate analysis maps reveal the same relationships of negative correlations between LST and tree cover and positive correlations between LST and impervious cover (Appendix C). While this relationship is dominantly linear between LST and impervious cover, the relationship appears to be non-linear for LST and tree cover. Many census tracts show a convexly negative relationship between tree cover and LST. In order to study this relationship further, the team plotted all census tracts for LST vs tree cover and LST vs impervious cover. The relationship between LST and impervious cover proved to be linear with an R^2 of 0.6 while the relationship between LST and tree cover proved to be logarithmic with an R^2 of 0.4 (Figure 6), where R^2 values closer to 1 indicate a better fit of the trendline. The fact that LST decreases logarithmically with increasing tree cover suggests that small increases in tree cover can have outsized effects on

temperature in census tracts with low tree cover (between 0 and 10%). On the other hand, efforts to increase tree cover past 40 or 50% may not substantially decrease LST. The linear relationship between LST and impervious surface cover suggests that temperatures continually increase as impervious surface cover increases rather than plateauing, at least up to roughly 80% impervious surface cover.

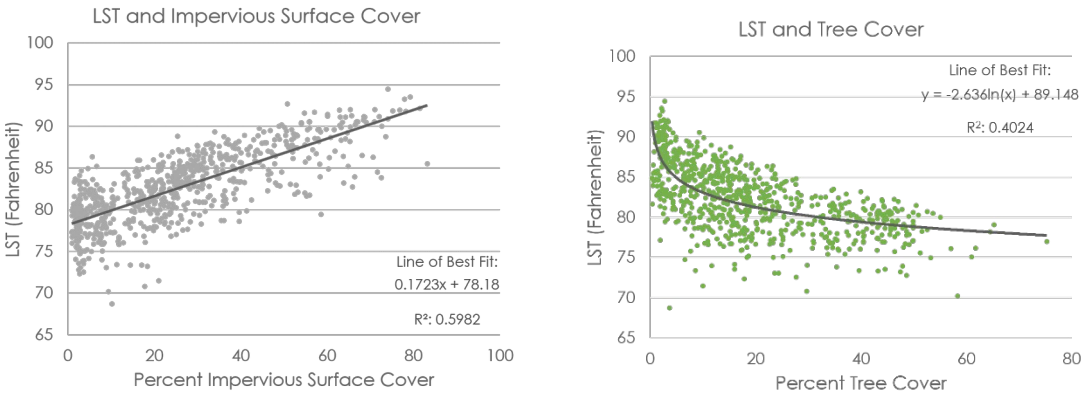

Figure 6. Plotted LST vs impervious cover and LST vs tree cover with their respective relationships.

4.1.2 Heat Vulnerability

The Heat Vulnerability Index indicated that the census tracts with the highest vulnerability to heat related illnesses are tracts 7.02 and 12, located just north and west of downtown respectively (Figure 7). The team found that these two tracts have experienced a 4 to 6 degree increase in LST since 2010 despite having a 2% increase in tree cover during the same time period. In the multivariate cluster analysis, the team found that tracts with the highest vulnerability happened to be in Cluster 3 which displays low tree cover and high impervious cover along with high LST. The team found that tract 105.02, located to the northwest of Huntsville city boundaries, and tract 18.01, located to the east of downtown, had the lowest vulnerability. These tracts saw an increase in tree cover of 6% and an increase in LST of 2-4 degrees for tract 105.02 and 4-6 degrees for tract 18.01.

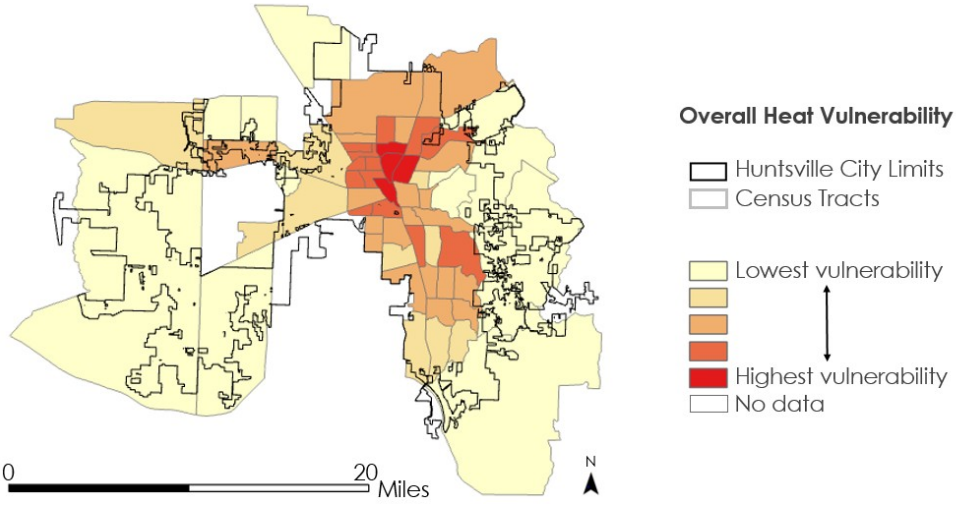

Figure 7. Urban Heat Health Risk Map showcasing Heat Vulnerability Index values by census tract.

4.1.3 Tree Canopy Survey

The ISS GEDI instrument detected a range of tree heights from 20 feet to 200 feet tall. This included transects that crossed through Monte Sano State Park. The average height of the tree canopy in the Huntsville area was 82 feet while the average plant area index was 3. GEDI transects were primarily limited to southeast and northwest Huntsville because the GEDI mission is only half-way through its two yearlong mission. A notable relationship displayed by GEDI data is the impact that tree cover has on LST. Plotting the tree heights over an LST map shows how effective trees are at cooling the surrounding land. An area in southwest Huntsville highlights this relationship as tree cover cuts through high LST and acts as nature's air conditioner (Figure 8).

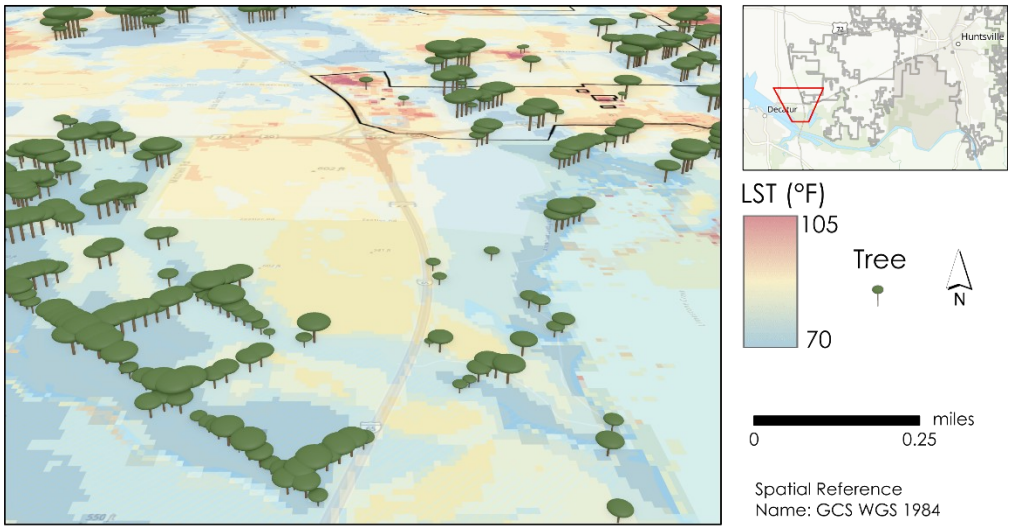

Figure 8. Spatial relationship of tree canopy cover and LST.

4.1.4 UHI Identification

The UHI Identification product consisted of maps showing average LST for summer 2019 using Landsat 8 TIRS along with a daytime and nighttime LST comparison using ISS ECOSTRESS for daytime LST and Terra MODIS for nighttime LST (Figure 9). The day and night LST comparison shows that the UHI effect not only has an effect during the daytime, but it can continue throughout the night. This can be seen through observing the areas with the highest LST during the day and how those areas retain the highest LST throughout the night.

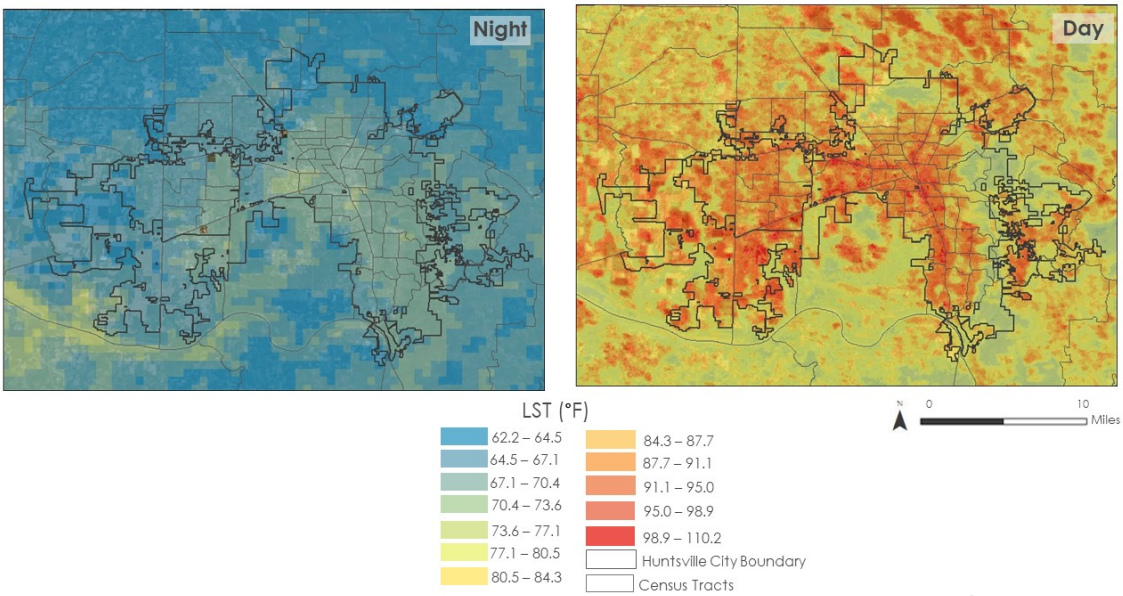

Figure 9. Daytime and Nighttime LST Comparison for June 12th, 2020.

The team overlaid the city of Huntsville census tracts on these images to allow viewers to observe LST in different locations throughout the city. The team observed average LST for summer 2019 more closely by selecting census tracts that were deemed important by partners (Figure 10). The team repeated this process for the day and night LST maps as well (Appendix F), and Census Tract 31 which lies within downtown Huntsville consistently appeared to demonstrate the highest LST values throughout all of the UHI Identification Maps.

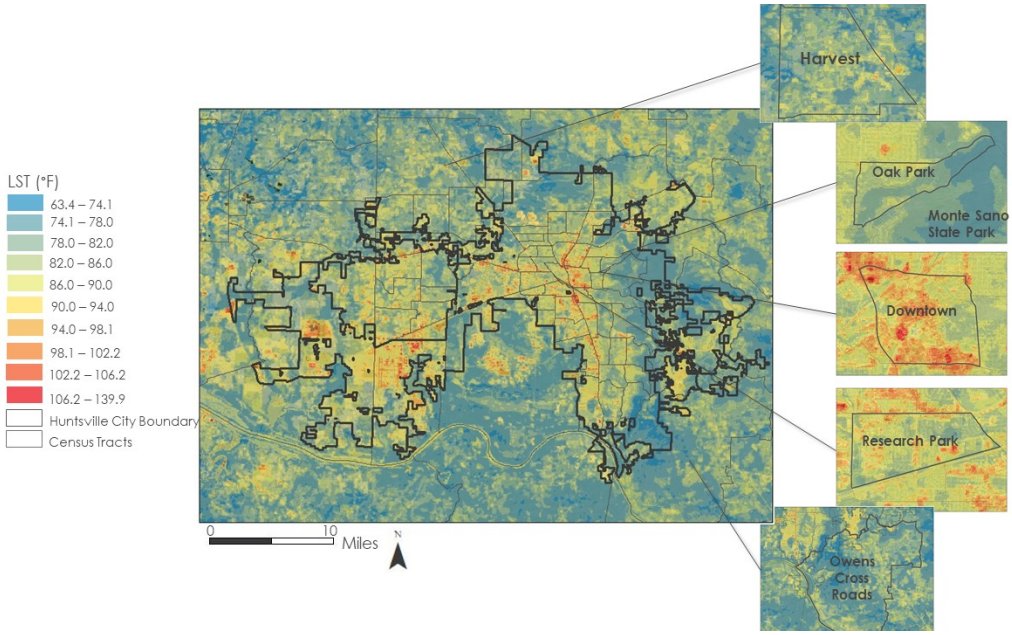

Figure 10. Average LST for Summer of 2019 in City of Huntsville Census Tracts.

4.2 Future Work

Future work could include a more detailed analysis of land cover types, including additional land cover classes. Given that two key processes associated with urban expansion (the expansion of impervious surface cover and the loss of urban trees) also threaten to intensify flood events, the City of Huntsville may benefit from additional research into the areas at most risk for flooding. Furthermore, future research could focus on performing similar analyses at a higher spatial resolution, potentially utilizing high-resolution LiDAR imagery with object-based image analysis, to allow for more targeted responses to urban heat hotspots (MacFaden et al., 2012).

5. Conclusions

The City of Huntsville can benefit from incorporating NASA EOs into its urban planning decision-making processes to alleviate the health risks posed by increasing LST. The team discovered that LST has increased by approximately 4 °F even while tree cover has increased by 3% across the city from 2010 to 2019. The resultant increasing tree canopy cover suggests that urban expansion in Huntsville has not substantially impacted tree canopy cover since 2010, although there may be more localized areas of tree cover loss due to development. The data also show that LST increases linearly with impervious surface and decreases logarithmically with tree cover. Therefore, tree cover has the potential to effectively mitigate the UHI effect in Huntsville, especially in the census tracts with very little tree cover and high impervious cover. Downtown Huntsville and the Huntsville International Airport both had the highest LST and highest percent of developed area. North Downtown Huntsville specifically had one of the highest heat vulnerability scores due to its high heat exposure and health vulnerability. Continuously monitoring changing tree canopy cover while prioritizing the placement of key green infrastructure is critical to planning for future urban growth in Huntsville, AL.

6. Acknowledgments

The Summer 2020 NASA DEVELOP Huntsville Urban Development team would like to thank our project partners at the City of Huntsville: Shane Davis, Francis Akridge, Sarah Powell, Lady Kassama, Amy Kenum, Nicholas Haney, Joy McKee, Ken Newberry, Kathy Martin, Gary Gleason, and Marc Byers. The team would also like to thank our science advisors, Dr. Robert Giffin and Dr. Jeffrey Luvall. We are also grateful to the guidance of our mentors Madison Murphy, Helen Baldwin, and Christine Evans, and our fellow A.R. Williams.

Any opinions, findings, and conclusions or recommendations expressed in this material are those of the author(s) and do not necessarily reflect the views of the National Aeronautics and Space Administration.

This material is based upon work supported by NASA through contract NNL16AA05C.

7. Glossary

BT – Brightness Temperature
Earth observations – Satellites and sensors that collect information about the Earth’s physical, chemical, and biological systems over space and time

CBER – Center for Business and Economic Research; an outreach unit within the Culverhouse College of Business at the University of Alabama created to promote Alabama's economic development by providing insight (data and analysis) through research and public service
CDC – Centers for Disease Control
EPA – Environmental Protection Agency
GEDI - Global Ecosystem Dynamics Investigation
GEE – Google Earth Engine
LiDAR – Light Detection and Ranging; technique in remote sensing that uses light in the form of a pulsed laser to measure variable distances to the Earth
LST – Land Surface Temperature
MODIS – Moderate Resolution Spectroradiometer
NDBI – Normalized Difference Built Up Index; indicates urban areas from the high reflectance of shortwave infrared light
NDVI – Normalized Difference Vegetation Index; an index of land cover measuring vegetation greenness
OLS – Ordinary Least Squares; linear least squares method for estimating an unknown parameter
SAR – Spatial Autoregression; a linear fit model correcting for autoregressive error or spatial lag
UHI effect – Urban heat island effect; caused by urban development involving the replacement of forested areas with impervious surfaces such as asphalt or concrete which hold onto heat, raising temperatures in more urban areas in comparison with the surrounding forested areas

8. References

Center for Business and Economic Research. (2020) "Alabama Economic Outlook 2020." The University of Alabama. https://hsvchamber.org/wp-content/uploads/2020/01/2020-Economic-Outlook-Huntsville-Metro-Area.pdf

City of Huntsville Urban Development, Long-Range Planning Division. (2020). "The Huntsville Development Review." 36. https://3jzi0q2zthm01oqpx2h96lz1-wpengine.netdna-ssl.com/wp-content/uploads/2020/01/HDR-Final-2019-C.pdfDubayah, R., Tang, H., Armston, J., Luthcke, S., Hofton, M., J. B. Blair (2020). GEDI L2B Canopy Cover and Vertical Profile Metrics Data Global Footprint Level V001 [Data set]. NASA EOSDIS Land Processes DAAC. https://doi.org/10.5067/GEDI/GEDI02_B.001

Dubayah, R., Tang, H., Armston, J., Luthcke, S., Hofton, M., J. B. Blair (2020). GEDI L2B Canopy Cover and Vertical Profile Metrics Data Global Footprint Level V001 [Data set]. NASA EOSDIS Land Processes DAAC. https://doi.org/10.5067/GEDI/GEDI02_B.001

Earthdata Search. (2019). Greenbelt, MD: Earth Science Data and Information System (ESDIS) Project, Earth Science Projects Division (ESPD), Flight Projects Directorate, Goddard Space Flight Center (GSFC) National Aeronautics and Space Administration (NASA). https://search.earthdata.nasa.gov/

Grover, A. & Singh, R. B. (2015). Analysis of urban heat island (UHI) in relation to normalized difference vegetation index (NDVI): A comparative study of Delhi and Mumbai. *Environments, 2*(2), 125-138. https://doi.org/10.3390/environments2020125

Hook, S. & Hulley, G. (2019). ECOSTRESS Land Surface Temperature and Emissivity Daily L2 Global 70 m V001 [Data set]. NASA EOSDIS Land Processes DAAC. Accessed 2020-06-25 from https://doi.org/10.5067/ECOSTRESS/ECO2LSTE.001

Imhoff, M. L., Zhang, P., Wolfe, R. E., & Bounoua, L. (2010). Remote sensing of the urban heat island effect across biomes in the continental USA. *Remote Sensing of Environment, 114*(3), 504-513. https://doi.org/10.1016/j.rse.2009.10.008

Keeratikasikorn, C., & Bonafoni, S. (2018). Urban heat island analysis over the land use zoning plan of Bangkok by means of Landsat 8 imagery. *Remote Sensing, 10*(3), 440. https://doi.org/10.3390/rs10030440

Kleerekoper, L., Van Esch, M., & Salcedo, T. B. (2012). How to make a city climate-proof, addressing the urban heat island effect. Resources, *Conservation and Recycling, 64*, 30-38. https://doi.org/10.1016/j.resconrec.2011.06.004

Kravcík M, Pokorny, Kohutiar J, Kovác M, Tóth E. (2009, June). Water for the Recovery of the Climate – A New Water Paradigm. Paper presented at the meeting Water as a Vulnerable and Exhaustible Resource, Prague.

Lo, C. P., Quattrochi, D. A., & Luvall, J. C. (1997). Application of high-resolution thermal infrared remote sensing and GIS to assess the urban heat island effect. *International Journal of Remote Sensing*, *18*(2), 287-304. https://doi.org/10.1080/014311697219079

Ossola, A., & Hopton, M. E. (2018). Measuring urban tree loss dynamics across residential landscapes. *Science of the Total Environment*, *612*, 940-949. https://doi.org/10.1016/j.scitotenv.2017.08.103

Macarof, P., & Statescu, F. (2017). Comparasion of NDBI and NDVI as indicators of surface urban heat island effect in Landsat 8 imagery: a case study of Iasi. *Present Environment and Sustainable Development, 11*(2), 141-150. https://doi.org/10.1515/pesd-2017-0032

MacFaden, S. W., O'Neil-Dunne, J. P., Royar, A. R., Lu, J. W., & Rundle, A. G. (2012). High-resolution tree canopy mapping for New York City using LIDAR and object-based image analysis. *Journal of Applied Remote Sensing*, 6(1), 063567. https://doi.org/10.1117/1.JRS.6.063567

Nowak, D. J. (2007). Assessing urban forest effects and values: New York City's urban forest (Vol. 9). US Department of Agriculture, Forest Service, Northern Research Station. https://doi.org/10.2737/NRS-RB-9

R Core Team (2020). R: A language and environment for statistical computing. R Foundation for Statistical Computing, Vienna, Austria. R version 4.0.0. https://www.R-project.org/

RStudio Team (2020). RStudio: Integrated Development Environment for R. RStudio, PBC, Boston, MA. R Studio version 1.3.956. http://www.rstudio.com/

Reid, C.E., Mann, J.K., Alfasso, R., English, P.B., King, G.C., Lincoln, R.A., Margolis, H.G., Rubado, D.J., Sabato, J.E., West, N.L., Woods, B., Navarro, K.M. & Balmes, J.R. (2012). Evaluation of a heat vulnerability index on abnormally hot days: An environmental public health tracking study. *Environmental Health Perspectives, 120(5)*, 715–720. https://doi.org/10.1289/ehp.1103766

Shen, H., Huang, L., Zhang, L., Wu, P., & Zeng, C. (2016). Long-term and fine-scale satellite monitoring of the urban heat island effect by the fusion of multi-temporal and multi-sensor remote sensed data: A 26-year case study of the city of Wuhan in China. *Remote Sensing of Environment*, *172*, 109-125. https://doi.org/10.1016/j.rse.2015.11.005

Silva, C.A., Hamamura, C., Valbuena, R., Hancock, S., Cardil, A., Broadbent, E. N., Almeida, D.R.A., Silva Junior, C.H.L, Klauberg, C. (2020). rGEDI: NASA's Global Ecosystem Dynamics Investigation (GEDI) Data Visualization and Processing. R package version 0.1.2. https://CRAN.R-project.org/package=rGEDI

Stone Jr, B., & Rodgers, M. O. (2001). Urban form and thermal efficiency: how the design of cities influences the urban heat island effect. American Planning Association. *Journal of the American Planning Association, 67*(2), 186. https://doi.org/10.1080/01944360108976228

United States Environmental Protection Agency. (2015, October 1). Reduce Urban Heat Island Effect [Overviews and Factsheets]. US EPA. https://www.epa.gov/green-infrastructure/reduce-urban-heat-island-effect

U.S. Geological Survey Earth Resources Observation and Science Center. (2012). Landsat TM Level-2 Surface Reflectance (SR) Science Product. U.S. Geological Survey. https://doi.org/10.5066/f7kd1vz9

U.S. Geological Survey Earth Resources Observations and Science Center. (2019). Landsat OLI/TIRS Level-2 Surface Reflectance (SR). Science Product. U.S. Geological Survey. https://doi.org/10.5066/f78s4mzj

Wan, Z., Hook, S., Hulley, G. (2015). MOD11A1 MODIS/Terra Land Surface Temperature/Emissivity Daily L3 Global 1km SIN Grid V006 [Data set]. NASA EOSDIS Land Processes DAAC. Accessed 2020-07-29 from https://doi.org/10.5067/MODIS/MOD11A1.006

Zhang, Y., Odeh, I. O., & Han, C. (2009). Bi-temporal characterization of land surface temperature in relation to impervious surface area, NDVI and NDBI, using a sub-pixel image analysis. *International Journal of Applied Earth Observation and Geoinformation*, *11*(4), 256-264. https://doi.org/10.1016/j.jag.2009.03.001

9. Appendices

Appendix A: Confusion Matrices

Table A1

Confusion Matrix: 2017 Supervised Classification, NAIP Imagery, 152 points

	Reference (NAIP)			
	Tree	Other	Develope	Water

			Pervious	d	
Supervised Classification	Tree	41	8	1	0
	Other Pervious	19	51	6	0
	Developed	0	6	9	0
	Water	5	1	0	5

Table A2
Confusion Matrix: 2011 Supervised Classification, NAIP Imagery, 152 points

		Reference (NAIP)			
		Tree	Other Pervious	Developed	Water
Supervised Classification	Tree	39	2	0	0
	Other Pervious	18	55	6	0
	Developed	4	7	9	0
	Water	6	0	0	5

Table A3
Confusion Matrix: 2011 Threshold Classification, NAIP Imagery, 152 points

		Reference (NAIP)			
		Tree	Other Pervious	Developed	Water
Threshold Classification	Tree	44	11	0	0
	Other Pervious	16	33	3	0
	Developed	7	21	12	4
	Water	0	0	0	1

Table A4
Confusion Matrix: 2017 Threshold Classification, NAIP Imagery, 152 points

		Reference (NAIP)			
		Tree	Other Pervious	Developed	Water
Threshold Classification	Tree	53	38	1	0
	Other Pervious	10	15	6	0
	Developed	2	13	9	1
	Water	0	0	0	4

Table A5
Confusion Matrix: 2016 Supervised Classification, NLCD Land Cover, 5000 points

	Reference (NLCD)

		Tree	Other Pervious	Developed	Water
Supervised Classification	Tree	1025	204	13	89
	Other Pervious	196	2136	115	29
	Developed	14	263	310	6
	Water	287	88	6	209

Table A6

Confusion Matrix: 2011 Supervised Classification, NLCD Land Cover, 5000 points

		Reference (NLCD)			
		Tree	Other Pervious	Developed	Water
Supervised Classification	Tree	1053	187	6	80
	Other Pervious	146	2211	113	32
	Developed	16	247	300	6
	Water	324	80	6	187

Appendix B: Spatial Autoregression

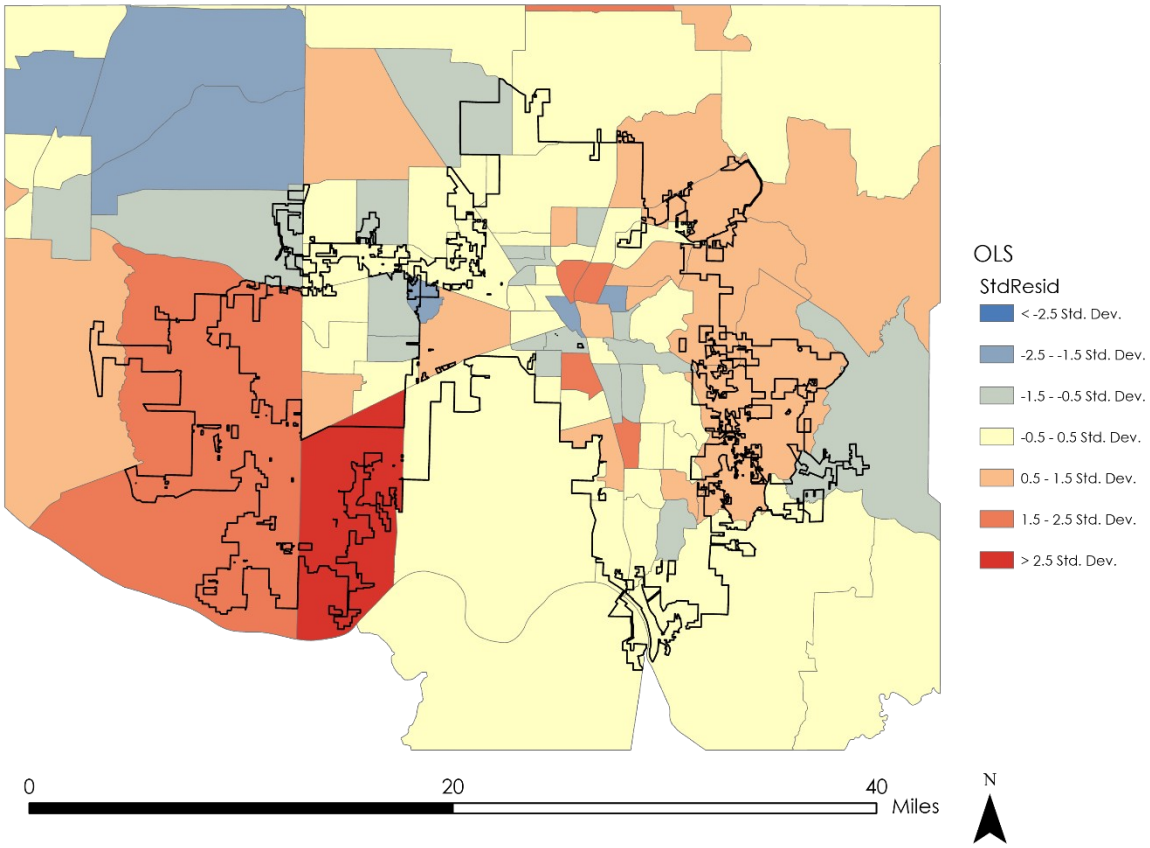

Figure B. Error corrected spatial autoregression (SAR) map displaying average LST values per census tract which were above (red) or below (blue) a predicted LST value given their respective percentage of impervious cover and tree cover.

Appendix C: Bivariate Analysis

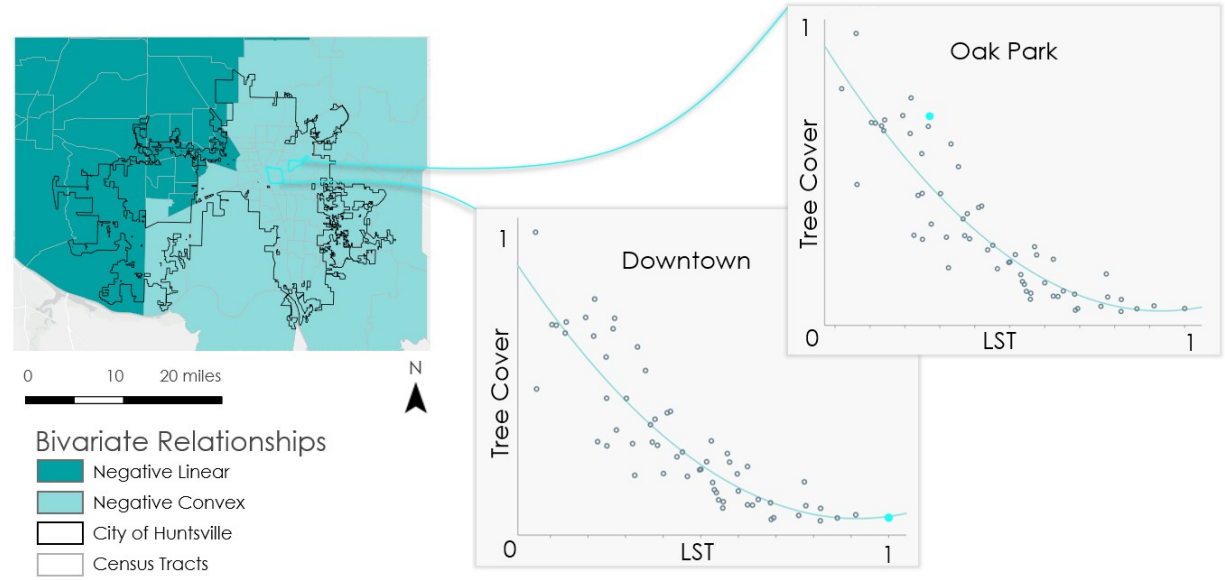

Figure C1. Local bivariate analysis for 60 of the nearest census tracts. Generally, as tree cover increases, LST decreases in a linear or convex slope. Downtown has high LST and low tree cover while Oak Park has low LST and high tree cover.

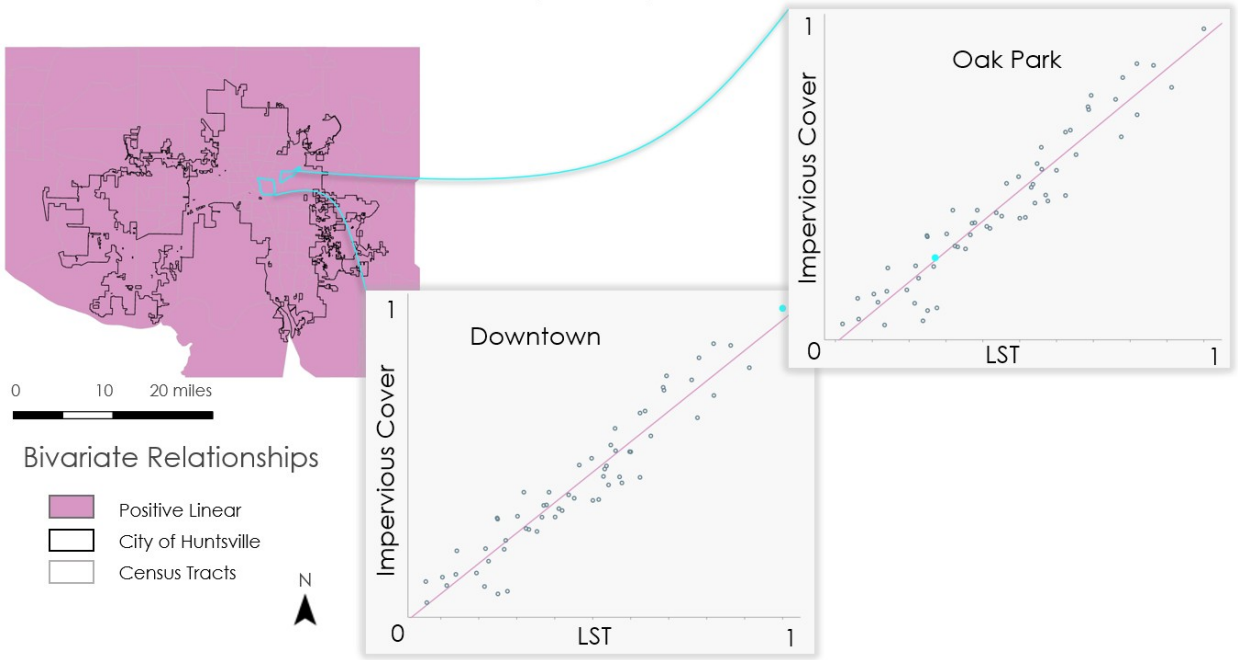

Figure C2. Local bivariate analysis for 60 of the nearest census tracts. Generally, as impervious cover increases, LST increases in a linear slope. Downtown has high LST and high impervious cover while Oak Park has low LST and low impervious cover.

Appendix D: Timeseries Graphs of Individual Census Tracts

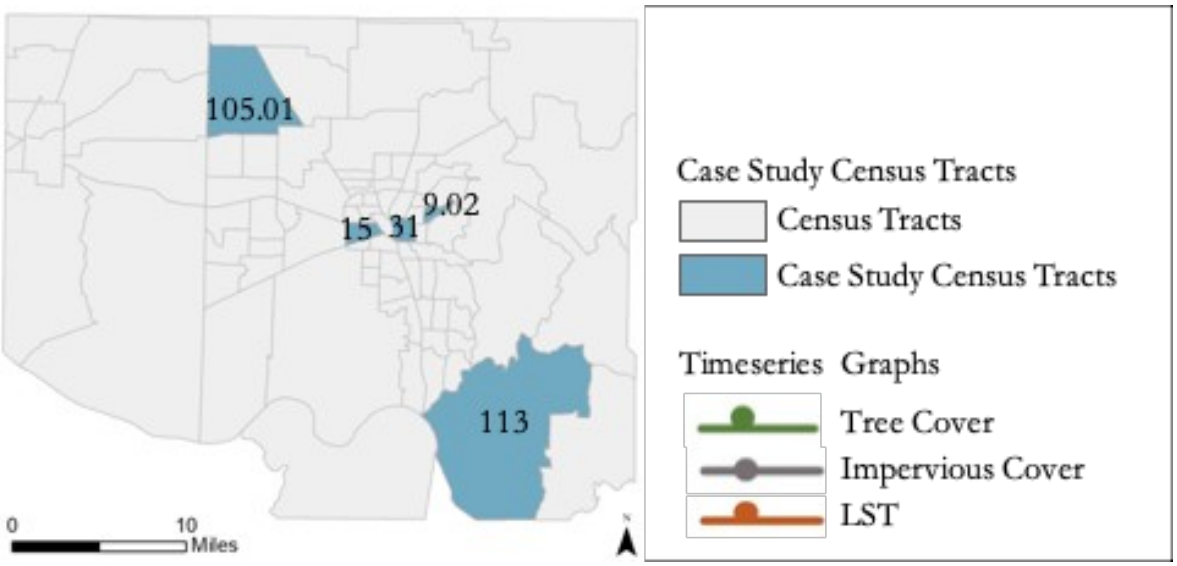

Figure D1. Case Study Census Tracts, with labels representing Census Tract numbers.

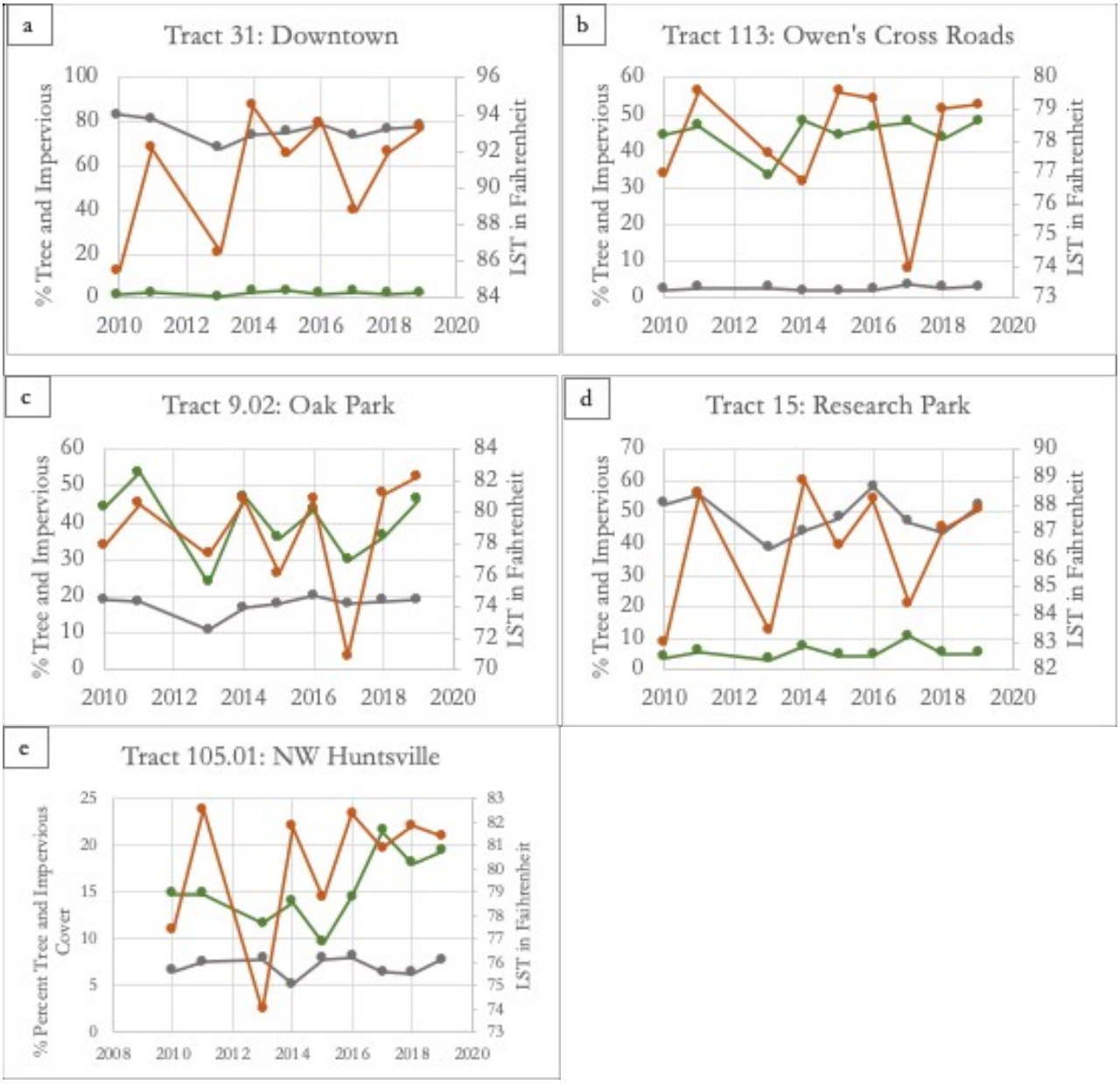

Figure D2. Case Study Census Tract Timeseries for Tracts 31 (a), 113 (b), 9.02 (c), 15 (d), and 105.01 (e)

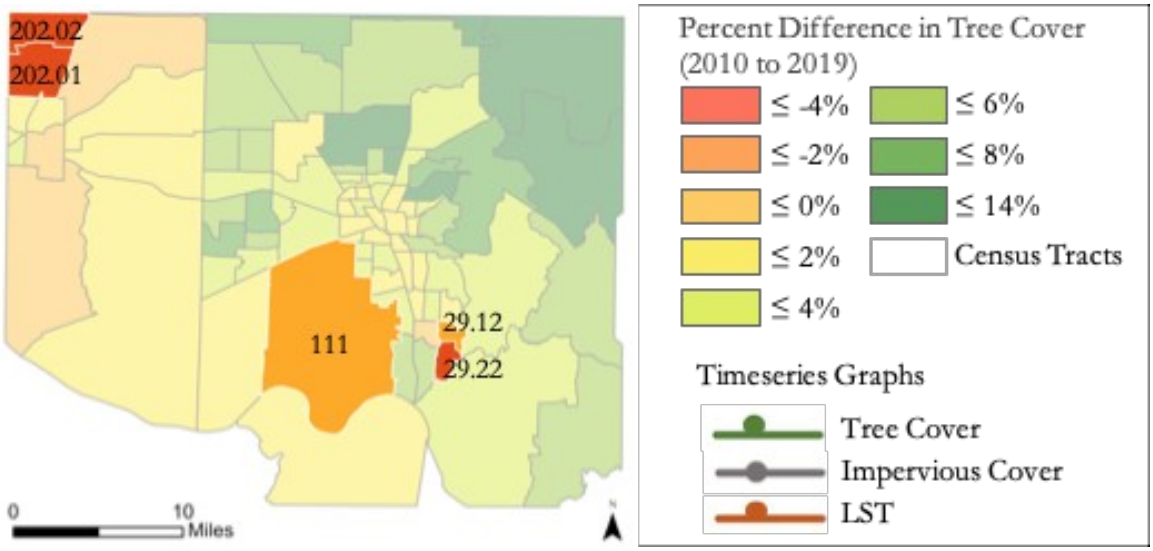

Figure D3. Census Tracts with the Most Tree Cover Loss, with labels representing Census Tract numbers.

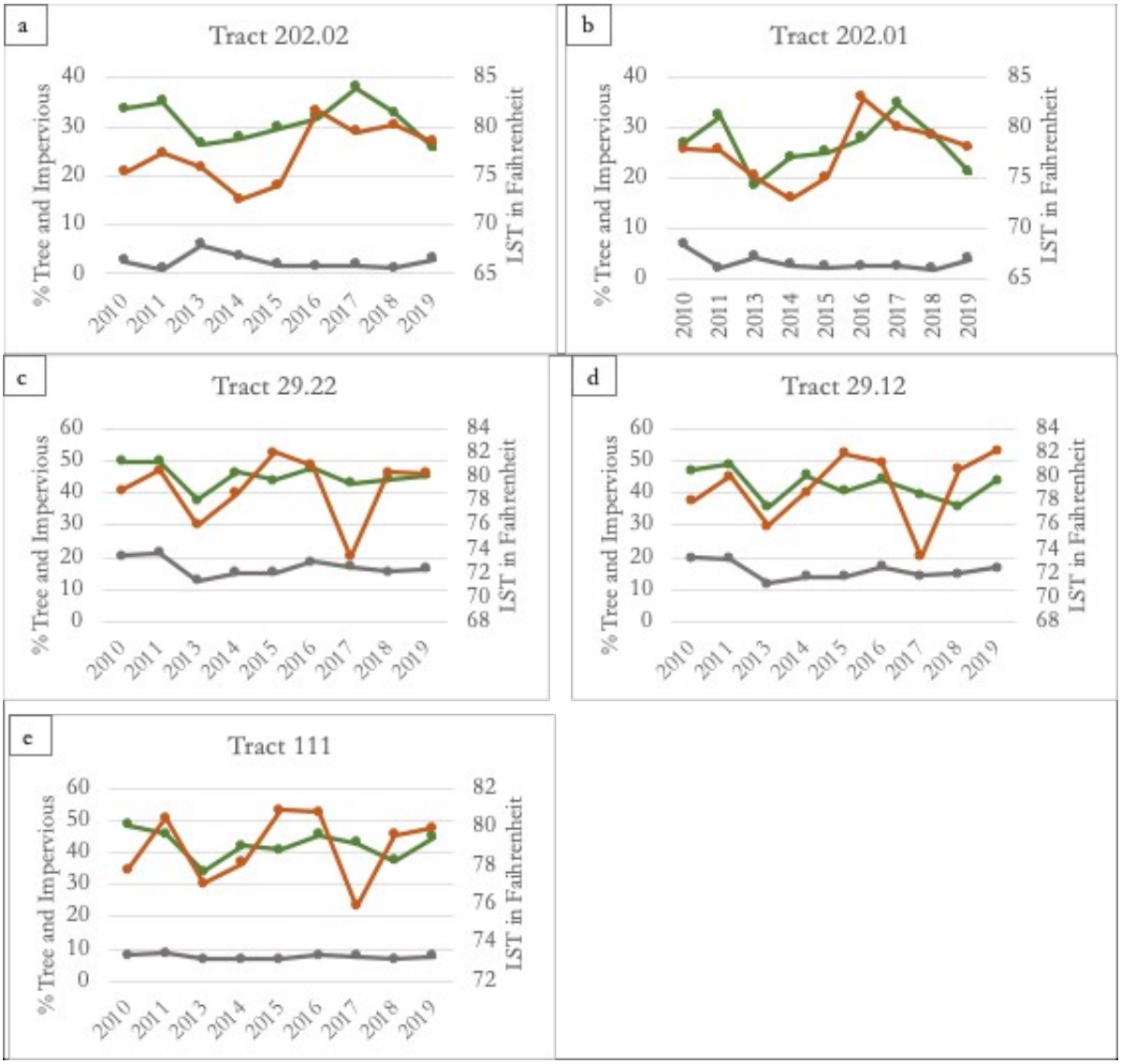

Figure D4. Timeseries Graphs for Tracts with Most Tree Cover Loss for Tracts 202.02 (a), 202.01 (b), 29.22 (c), 29.12 (d), 111(e)

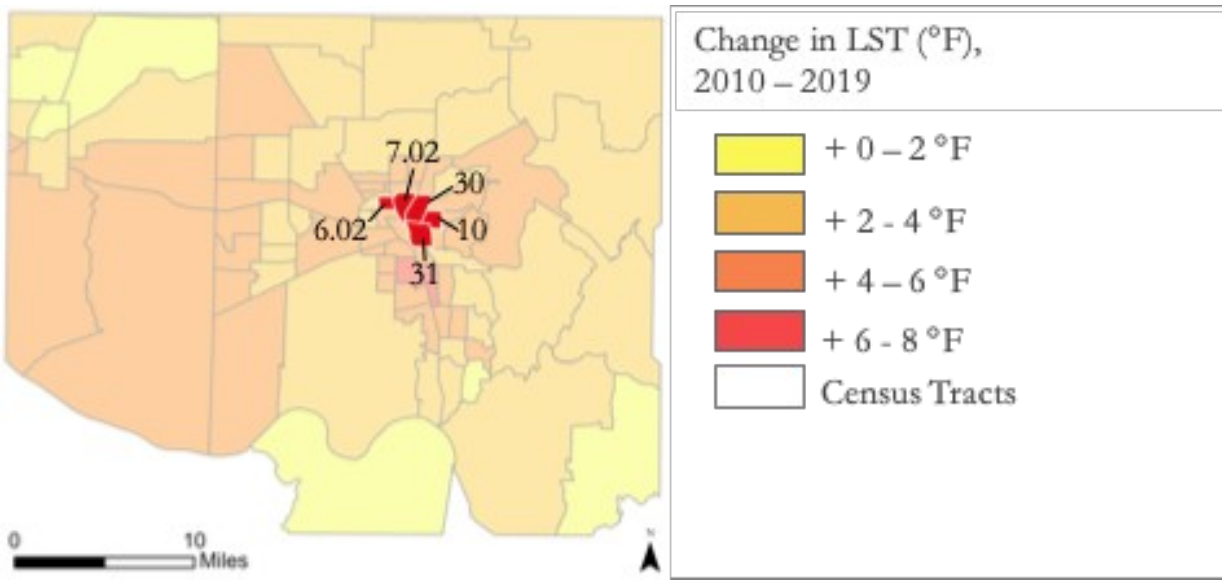

Figure D5. Tracts with Highest LST Increase, with labels representing Census Tract numbers.

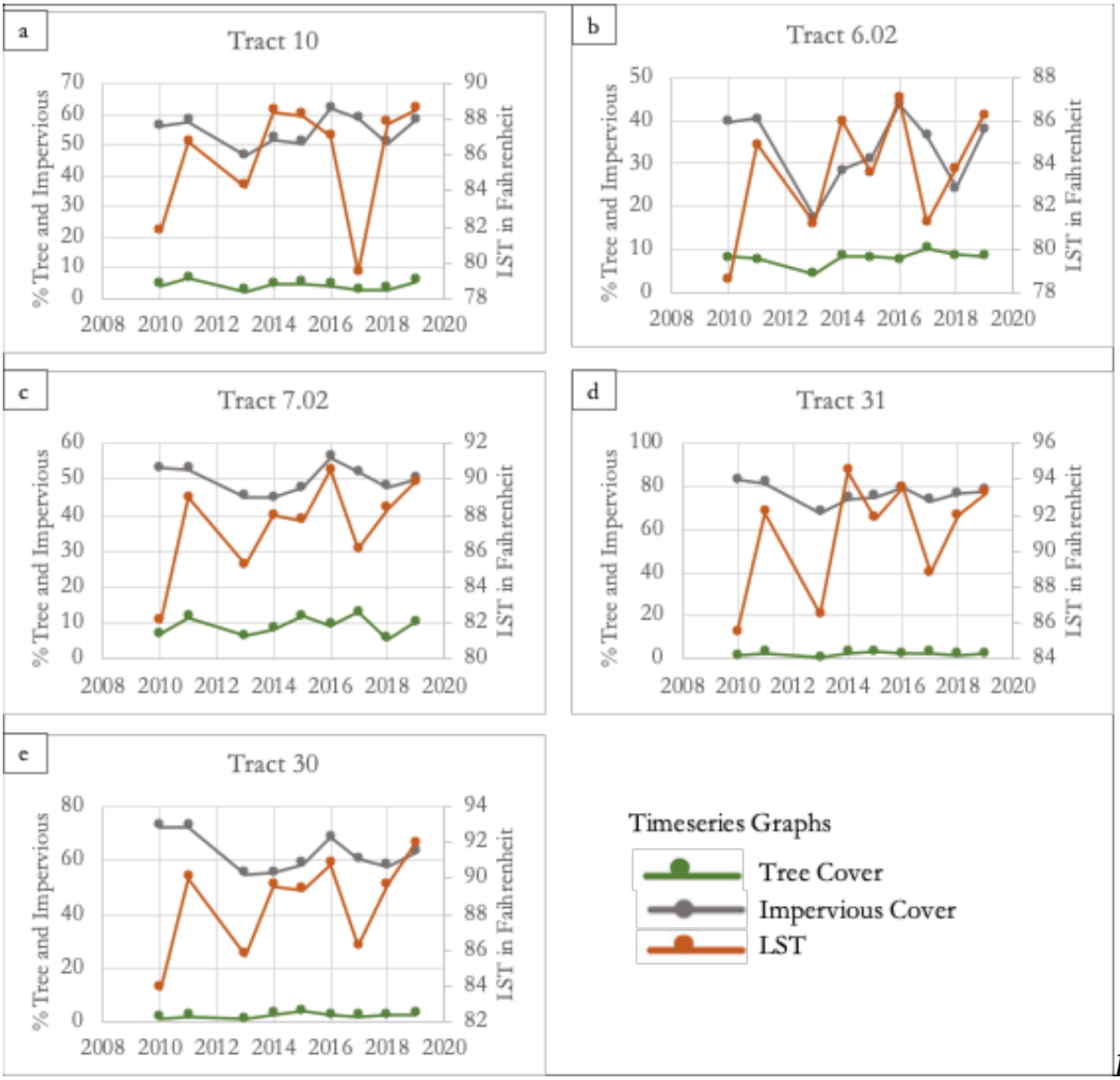

Figure D6. Timeseries Graphs for Tracts with Most LST Increase for Tracts 10 (a), 6.02 (b), 7.02 (c), 31 (d), 30 (e)

Appendix F. UHI Identification: Day and Night LST Maps

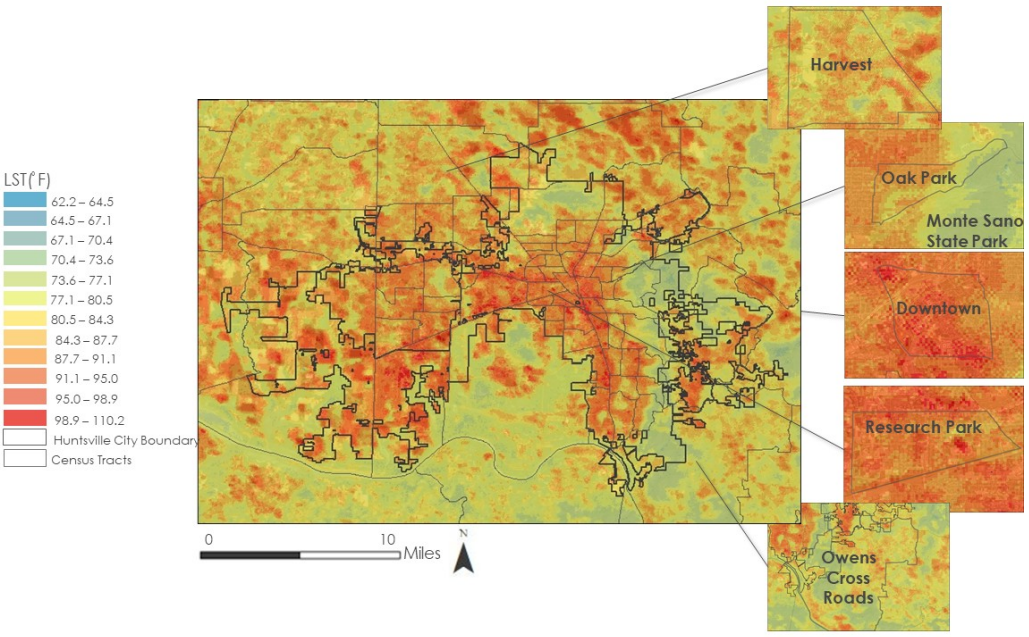

Figure F1. Daytime LST for City of Huntsville Census Tracts for June 12th, 2020

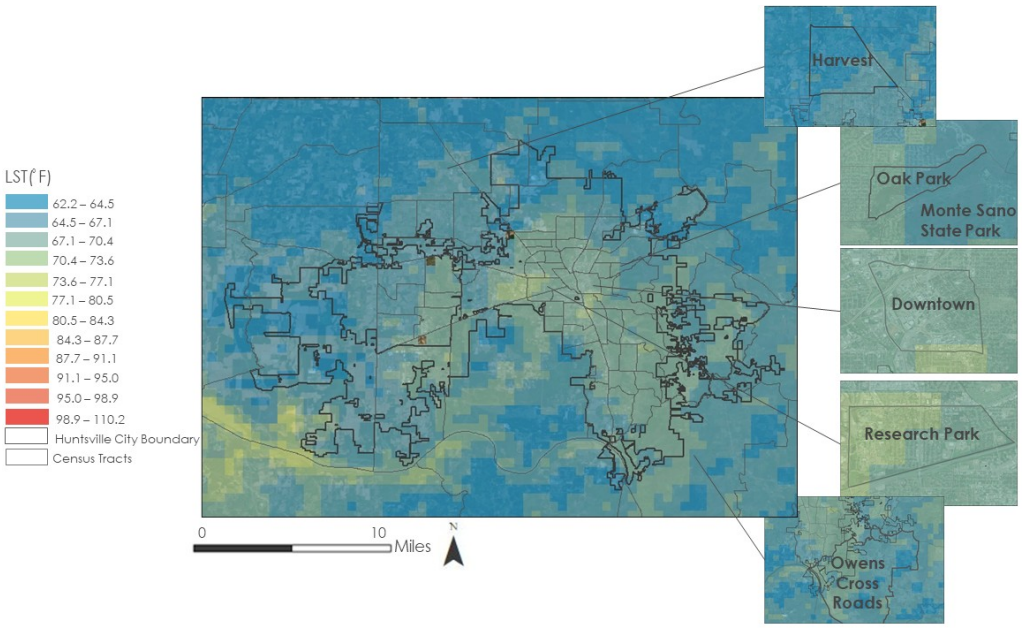

Figure F2. Nighttime LST for City of Huntsville Census Tracts for June 12th, 2020